Numerical investigation of relative intensity noise in frequency-doubled multimode fiber lasers

Rodolphe Collin, Thierry Chartier, Pascal Besnard

Version of Record: https://www.sciencedirect.com/science/article/pii/S0030401820311433
Manuscript_22cb98bcd90da44050c9d6a87c6ba315

Numerical investigation of relative intensity noise in frequency-doubled multimode fiber lasers

Rodolphe Collin, Thierry Chartier, Pascal Besnard

Univ Rennes, CNRS, Institut FOTON - UMR 6082, F-22305 Lannion, France

Abstract

In this paper, we study the intensity noise performance of frequency-doubled lasers. In particular, we investigate how the relative intensity noise (RIN) of multimode fiber lasers is affected by the second harmonic generation process. We first develop an analytical approach and show that, in contrast with a single-mode laser, the low frequency RIN (or excess noise) of a two-mode laser can increase of more than 6 dB after the frequency-doubling operation. This occurs when the intensities of both modes are different and this is explained by a nonlinear coupling between noise and intensity of modes. To deal with more commonly-used multimode fiber lasers, we have extended our study to any number of modes. For this purpose, we have developed a model to numerically simulate the dynamics of a multimode fiber laser. This model includes noise sources and mode competition dynamics due to spatial hole burning. It gives access to the complex amplitude of the electric field of the laser. Using this model, we have confirmed that the excess noise of frequency-doubled multimode fiber lasers can be more than 6 dB higher than the excess noise of the laser before frequency-doubling.

Keywords: Multimode laser, Fiber laser, Relative intensity noise, Second harmonic generation, Mode competition.

1. Introduction

High power visible laser sources are of great interest for many applications. Since there is no high-power amplifier in the visible range, high-power visible lasers are generally frequency-doubled near-infrared lasers. Yb-doped fiber lasers, operating around 1060 nm, are good candidates to realize green lasers around 530 nm. In the past decades, high-power Yb-doped fiber lasers have known a

large development [1]. Using these types of lasers, in association with second-order nonlinear effects, high-power green lasers have been demonstrated [2, 3]. Nowadays, frequency-doubled fiber lasers are commonly used as laser sources, delivering several tens of watts of average power in the visible range.

In the continuous-wave (CW) operating regime, good stability of the visible laser emission is sometimes required in some applications. This has led to numerous studies on the influence of nonlinear effects on the phase or intensity noise of such lasers. For example, the "green noise" of multimode frequency-doubled lasers is attributed to power fluctuations between modes due to the intracavity second-harmonic generation (SHG) process. On the other hand, nonlinear effects can also be used to lower the intensity noise of intracavity frequency-doubled laser sources [4, 5].

In frequency-doubled fiber lasers, the SHG process is generally performed outside the laser cavity and the green noise cannot occur. However, in some extra-cavity frequency-doubled lasers, an increase of the low-frequency relative intensity noise (RIN), up to 10 dB, has been observed after the frequency-doubling process [6, 7]. In Ref. [6], authors claim that it would be a consequence of the finite acceptance of the nonlinear crystal.

In this paper, we propose a new explanation of the increase of the low-frequency RIN of extra-cavity frequency-doubled multimode lasers. We show that there is no need to take into account any limitation of the nonlinear crystal. We simply take into account the multimode behavior of the laser and the squaring of the laser field due to the SHG process. In this paper, we also propose an original model to simulate the dynamics of multimode fiber lasers. This model consists in a set of time-derivative equations that include both the spatial hole burning effect (leading to mode competition) and the classical Langevin noise forces. Solving numerically these equations gives access to the complex amplitude of the electrical field of each mode. To the best of our knowledge, such a model, including both spatial hole burning and noise, is proposed for the first time in this paper. We apply this model to the case of a multimode Yb-doped fiber laser in order to investigate the effect of frequency doubling on the RIN of the laser.

The paper is organized as follows. In Section 2, we propose an analytical study of the RIN of the laser before and after the frequency-doubling process. We start by a single-mode laser and show that SHG always results in a 6 dB increase of the RIN of the laser. Then, we study the case of a two-mode laser. We derive an analytical formula that gives the conditions for which the increase of the RIN can be higher than 6 dB. In Section 3, we present the theoretical model that allows us to numerically study the RIN of a multimode Yb-doped fiber laser. In Section

4, we use the model to study the RIN of the Yb-doped fiber laser before and after SHG. The results confirm that the increase of the low-frequency RIN can be much greater than 6 dB for standard operating conditions of a fiber laser.

2. Analytical study of RIN after frequency doubling

In this section, we present analytical expressions to calculate the increase of the low-frequency RIN of a laser before and after a frequency-doubling process. We start by a single-mode laser, then, we study the case of a two-mode laser. The study of a laser with a larger number of modes will be performed numerically in Section 3.

2.1. Single-mode laser

Let us consider the electric field $E_\omega(t)$ of a single-mode CW laser at the fundamental frequency ω. The intensity $I_\omega(t)$ of the laser is defined by the following relation [8]

$$I_\omega(t) = \frac{nc\varepsilon_0}{2}|E_\omega(t)|^2, \tag{1}$$

where n is the refractive index of the medium in which light propagates, c the speed of light in vacuum and ε_0 the vacuum permittivity. We assume that the intensity $I_\omega(t)$ exhibits noise and can be written as

$$I_\omega(t) = \langle I_\omega \rangle + \delta I_\omega(t), \tag{2}$$

where $\langle I_\omega \rangle$ is the average value of $I_\omega(t)$ and $\delta I_\omega(t)$ its the time-dependent fluctuations around $\langle I_\omega \rangle$. We assume that the fluctuations are weak with respect to the average value, i.e. $\delta I_\omega(t) \ll \langle I_\omega \rangle$. The RIN of the laser is defined as follows [9]

$$\mathrm{RIN}_\omega(\nu) = \frac{\langle |\tilde{\delta} I_\omega(\nu)|^2 \rangle}{\langle I_\omega \rangle^2}, \tag{3}$$

where $\tilde{\delta} I_\omega(\nu)$ is the Fourier transform of the intensity fluctuations $\delta I_\omega(t)$. The quantity $\langle |\tilde{\delta} I_\omega(\nu)|^2 \rangle$ is usually referred to as the power spectral density (PSD) of the laser intensity noise.

We now assume that the SHG process leads to a frequency-doubled electric field $E_{2\omega}(t)$. In our approach, we simply write $E_{2\omega}(t)$ as the square of the fundamental electric field $E_\omega(t)$ [10]

$$E_{2\omega}(t) = \eta E_\omega^2(t), \tag{4}$$

where η is the efficiency of the SHG operation. Modeling the SHG operation by simply squaring the fundamental field is quite straightforward. The underlying assumptions are, for example, that wave planes are considered or that the phase-matching condition is satisfied. Even if these hypothesis are not fully satisfied in real systems, we want to focus here on the main effect of SHG, i.e. the squaring of the fundamental electric field.

Similarly to equation (1) for the initial field, the intensity of the doubled-frequency field writes

$$I_{2\omega}(t) = \frac{nc\varepsilon_0}{2}|E_{2\omega}(t)|^2. \tag{5}$$

Using relations (1), (2) and (4) in equation (5), the intensity $I_{2\omega}(t)$ of the frequency-doubled field can be written as

$$I_{2\omega}(t) = \langle I_\omega \rangle^2 + 2\langle I_\omega \rangle \delta I_\omega(t) + \delta I_\omega^2(t). \tag{6}$$

Since we have $\delta I_\omega(t) \ll \langle I_\omega \rangle$, we neglect the second-order term $\delta I_\omega^2(t)$ in equation (6). Then, we set

$$I_{2\omega}(t) = \langle I_{2\omega} \rangle + \delta I_{2\omega}(t), \tag{7}$$

with $\langle I_{2\omega} \rangle = \langle I_\omega \rangle^2$ and $\delta I_{2\omega}(t) = 2\langle I_\omega \rangle \delta I_\omega(t)$. The RIN of the frequency doubled laser is defined as follows

$$\mathrm{RIN}_{2\omega}(\nu) = \frac{\langle |\tilde{\delta} I_{2\omega}(\nu)|^2 \rangle}{\langle I_{2\omega} \rangle^2}. \tag{8}$$

Then, we obtain

$$\mathrm{RIN}_{2\omega}(\nu) = 4\frac{\langle |\tilde{\delta} I_{\omega}(\nu)|^2 \rangle}{\langle I_{\omega} \rangle^2} = 4\mathrm{RIN}_{\omega}(\nu). \tag{9}$$

Relation (9) shows mathematically that the RIN of a frequency-doubled CW single-mode laser is 6 dB higher than the RIN of the initial laser.

To illustrate this point, figure 1 plots the RIN of a typical CW single-mode fiber laser. In this figure, two cases are considered. In the first case, the pump power P_p is very close to the threshold P_{th} of the laser ($P_p = 1.05P_{\mathrm{th}}$). In the second case, the pump power is clearly above the threshold ($P_p = 2P_{\mathrm{th}}$). These curves have been obtained numerically from the model that will be detailed in Section 3. For each case, the RIN exhibits a constant value at low frequencies, usually referred to as the excess noise of the laser. This noise is due to the pump noise. The pronounced peak around few tens of kHz is the relaxation frequency of

the laser. At higher frequencies, the RIN drops down with a 40 dB/decade slope. The electric field at ω has been squared and the RIN of the frequency-doubled laser is also plotted in figure 1. As predicted by equation (9) we observe a 6 dB increase of the RIN through the SHG process. We also note that the RIN of the laser near threshold (first case) is higher than the RIN of the laser at twice the threshold (second case). This well-known result is explained by the fact that, near threshold, a laser exhibits more noise due to spontaneous emission.

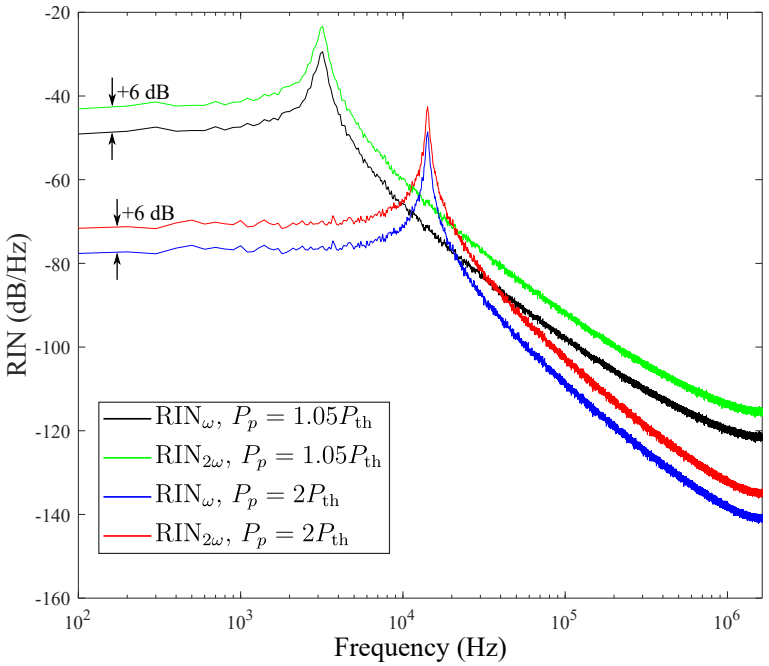

Figure 1: RIN of a single-mode laser before and after frequency doubling, for two pumping levels: very close to threshold ($P_p = 1.05P_{\rm th}$) and twice above threshold ($P_p = 2P_{\rm th}$).

Finally, we note from figure 1 that the RIN of a typical CW single-mode fiber laser has its main contribution essentially at low frequencies (typically below 1 MHz).

2.2. Two-mode laser

In the case of a two-mode laser, we assume that the total electric field $E_\omega(t)$, around a fundamental frequency ω, is the sum of two electric fields $E_1(t)$ and $E_2(t)$ at different frequencies

$$E_\omega(t) = E_1(t) + E_2(t). \tag{10}$$

We write the electric fields $E_1(t)$ and $E_2(t)$ of each mode as follows

$$E_q(t) = \sqrt{\frac{2}{nc\varepsilon_0} I_q(t)} e^{i[\omega_q t + \theta_q(t)]}, \tag{11}$$

where $q = 1, 2$, $I_q(t)$ is the intensity of each mode, ω_q their angular frequency and $\theta_q(t)$ their phase. In the following, we neglect the phase noise and set $\theta_q(t) = 0$. We assume that the intensity of each mode weakly fluctuates around an average value and we set

$$I_q(t) = \langle I_q \rangle + \delta I_q(t), \tag{12}$$

where $\langle I_q \rangle$ represents the average value of $I_q(t)$ and $\delta I_q(t)$ the fluctuations of $I_q(t)$ around its average value. Let us define the RIN of each mode independently

$$\mathrm{RIN}_q(\nu) = \frac{\langle |\tilde{\delta} I_q(\nu)|^2 \rangle}{\langle I_q \rangle^2}, \tag{13}$$

where $\tilde{\delta} I_q(\nu)$ is the Fourier transform of $\delta I_q(t)$. We consider that the RIN of each mode is similar to the RIN of figure 1 and expands only at low frequencies (typically below 1 MHz).

Using the definition of equation (1) for the intensity $I_\omega(t)$, we find the intensity of the two-mode laser

$$I_\omega(t) = I_1(t) + I_2(t) + 2\sqrt{I_1(t) I_2(t)} \cos[(\omega_1 - \omega_2)t]. \tag{14}$$

Equation (14) contains two different terms. The first term $I_1(t) + I_2(t)$ is the sum of both intensities of each mode. In the frequency domain, this term should only present fluctuations at low frequencies (typically below 1 MHz), similarly to figure 1. The intensity $I_\omega(t)$ also contains a beating term at the frequency difference $(\omega_1 - \omega_2)$. The mode frequencies differ from the free spectral range (FSR) of a laser cavity and the frequency difference $\Delta\nu = (\omega_1 - \omega_2)/2\pi$ is typically of the order of few MHz. In the frequency domain, this beating term leads to a frequency peak at the FSR of the cavity and then at a frequency much higher than the frequency range of $I_1(t) + I_2(t)$. In consequence, we decompose $I_\omega(t)$ in two distinct contributions, its low-frequency contribution $I_{\omega\mathrm{lf}}(t)$ and its high-frequency contribution $I_{\omega\mathrm{hf}}(t)$

$$I_\omega(t) = I_{\omega\mathrm{lf}}(t) + I_{\omega\mathrm{hf}}(t), \tag{15}$$

with

$$I_{\omega\mathrm{lf}}(t) = I_1(t) + I_2(t), \tag{16}$$

$$I_{\omega\mathrm{hf}}(t) = 2\sqrt{I_1(t) I_2(t)} \cos(\delta\omega t), \tag{17}$$

and $\delta\omega = \omega_1 - \omega_2$. The low-frequency intensity $I_{\omega\mathrm{lf}}(t)$ can be decomposed in its CW part $\langle I_{\omega\mathrm{lf}}\rangle$ and its time-dependent part $\delta I_{\omega\mathrm{lf}}(t)$

$$I_{\omega\mathrm{lf}}(t) = \langle I_{\omega\mathrm{lf}}\rangle + \delta I_{\omega\mathrm{lf}}(t), \tag{18}$$

with

$$\langle I_{\omega\mathrm{lf}}\rangle = \langle I_1\rangle + \langle I_2\rangle, \tag{19}$$

$$\delta I_{\omega\mathrm{lf}}(t) = \delta I_1(t) + \delta I_2(t). \tag{20}$$

If we assume that the fluctuations $\delta I_1(t)$ and $\delta I_2(t)$ on both modes are perfectly uncorrelated, a straightforward calculation shows that the PSD of the sum of the modes is equal to the sum of the PSD of each mode. This assumption is common in CW multimode fiber lasers with a large number of modes [11]. In the case of a two-mode laser, this assumption may not be satisfied. However, our goal is here to improve the understanding of real multimode fiber lasers with a large number of modes. Thus, for the sake of simplicity, we keep the assumption of uncorrelated modes, even for the particular case of a two-mode laser. Then, the low-frequency RIN of a two-mode laser writes

$$\mathrm{RIN}_{\omega\mathrm{lf}}(\nu) = \frac{\langle|\tilde{\delta I}_1(\nu)|^2\rangle + \langle|\tilde{\delta I}_2(\nu)|^2\rangle}{\left(\langle I_1\rangle + \langle I_2\rangle\right)^2}. \tag{21}$$

In order to calculate the low-frequency RIN of the frequency-doubled laser, we now calculate the intensity by using equations (4), (10) and (11)

$$\begin{aligned} I_{2\omega}(t) =& \eta\Big[I_1^2(t) + I_2^2(t) + 4I_1(t)I_2(t) \\ &+ 4I_1(t)\sqrt{I_1(t)I_2(t)}\cos(\delta\omega t) + 4I_2(t)\sqrt{I_1(t)I_2(t)}\cos(\delta\omega t) \\ &+ 2I_1(t)I_2(t)\cos(2\delta\omega t)\Big]. \end{aligned} \tag{22}$$

The frequency-doubled intensity exhibits two high-frequency peaks, at $\delta\omega$ and $2\delta\omega$ respectively. Similarly to the single-mode case, we decompose $I_{2\omega}(t)$ in its low-frequency contribution $I_{2\omega\mathrm{lf}}(t)$ and its high-frequency contribution $I_{2\omega\mathrm{hf}}(t)$

$$I_{2\omega\mathrm{lf}}(t) = \langle I_{2\omega\mathrm{lf}}\rangle + \delta I_{2\omega\mathrm{lf}}(t), \tag{23}$$

with

$$I_{2\omega\mathrm{lf}}(t) = \eta[I_1^2(t) + I_2^2(t) + 4I_1(t)I_2(t)], \tag{24}$$

$$\begin{aligned} I_{2\omega\mathrm{hf}}(t) =& \eta\Big[4I_1(t)\sqrt{I_1(t)I_2(t)}\cos(\delta\omega t) + 4I_2(t)\sqrt{I_1(t)I_2(t)}\cos(\delta\omega t) \\ &+ 2I_1(t)I_2(t)\cos(2\delta\omega t)\Big]. \end{aligned} \tag{25}$$

Using equation (12), we decompose $I_{2\omega\mathrm{lf}}(t)$ in its CW part $\langle I_{2\omega\mathrm{lf}}\rangle$ and its time-dependent part $\delta I_{2\omega\mathrm{lf}}(t)$. Then, after a straightforward calculation and the assumption of uncorrelated noises, it can be shown that the low-frequency RIN of the frequency-doubled two-mode laser can be expressed as follows

$$\mathrm{RIN}_{2\omega\mathrm{lf}}(\nu) = 4\frac{(\langle I_1\rangle + 2\langle I_2\rangle)^2\langle|\tilde{\delta}I_1(\nu)|^2\rangle + (2\langle I_1\rangle + \langle I_2\rangle)^2\langle|\tilde{\delta}I_2(\nu)|^2\rangle}{(\langle I_1\rangle^2 + \langle I_2\rangle^2 + 4\langle I_1\rangle\langle I_2\rangle)^2}. \quad (26)$$

The denominator of equation (26) depends only on the average intensities of the two modes but the numerator depends on both the average intensities and the fluctuations of the modes. Therefore, analysis of the frequency-doubled RIN is not as simple as in the single-mode case. To compare the low-frequency RINs of the two-mode laser before and after the frequency-doubling process, we define the ratio Γ between both RINs

$$\Gamma = \frac{\mathrm{RIN}_{2\omega\mathrm{lf}}}{\mathrm{RIN}_{\omega\mathrm{lf}}}. \quad (27)$$

We introduce the parameters γ and α, representing the ratio between the RINs of each individual mode and the ratio between the average intensities of each mode, respectively

$$\gamma = \frac{\mathrm{RIN}_1}{\mathrm{RIN}_2}, \quad (28)$$

$$\alpha = \frac{\langle I_1\rangle}{\langle I_2\rangle}. \quad (29)$$

Using these definitions, we can express Γ as a function of α and γ

$$\Gamma = 4\frac{[\gamma\alpha^2(2+\alpha)^2 + (1+2\alpha)^2](1+\alpha)^2}{(1+4\alpha+\alpha^2)^2(1+\gamma\alpha^2)}. \quad (30)$$

Figure 2 shows the evolution of Γ as a function of α for different values of γ (mentioned on the curves). First, we note that Γ is always greater than 0 dB. This means that the SHG process always impairs the low-frequency RIN of a two-mode laser, similarly to a single-mode laser for which we have found a 6 dB increase of the RIN. Secondly, we see that the increase of the RIN can be, under certain conditions, lower than 6 dB. It can also be higher than 6 dB. Let us now examine this point in more details.

First, when $\alpha = 0$ dB, the ratio Γ is 6dB, whatever the value of γ. This means that, when both modes have the same average intensity, the increase of

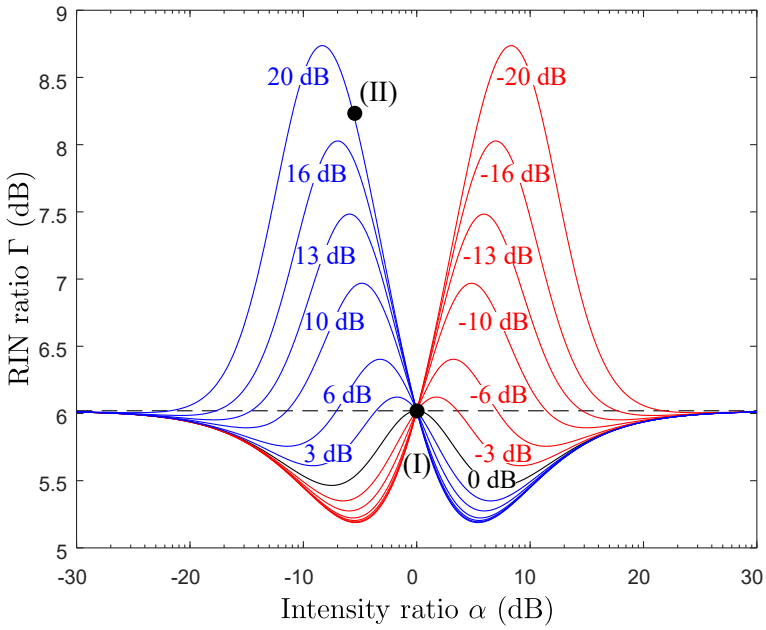

Figure 2: Evolution of the ratio Γ between the low-frequency RINs of a two mode laser, before and after SHG, as a function of the ratio α between the average intensities of each mode, for several values of the ratio γ between the RINs of each mode (mentioned on the curves). Points (I) and (II) will be introduced in Section 4.

the frequency-doubled RIN is always 6 dB, whatever the RIN of each individual mode.

Values of Γ greater than 6 dB occur if $\alpha < 0$ dB and $\gamma > 0$ dB or when $\alpha > 0$ dB and $\gamma < 0$ dB. This means that the increase of the frequency-doubled RIN can be more than 6 dB only if the weakest mode (the mode with the lowest average intensity) exhibits the highest RIN. This conclusion may be counter-intuitive if we expect that the weakest mode has a lower contribution to the total RIN than the strongest mode. However, this effect can be explained by equation (26). We see, at the numerator of this equation, that the fluctuations of one mode are multiplied by the average power of the other mode. This amplifies the strongest RIN through the power of the strongest mode and leads to an increase of the total RIN with a factor higher than in the single-mode case (6 dB). We note from figure 2 that, in these two cases ($\alpha < 0$ dB, $\gamma > 0$ dB and $\alpha > 0$ dB, $\gamma < 0$ dB), the increase Γ of the frequency-doubled RIN is not systematically higher than 6 dB. The value of Γ depends on the relative values of α and γ. For example, for a given value of α, the ratio γ must be strong enough to lead to a value of Γ greater than 6 dB.

In the other cases ($\alpha < 0$ dB and $\gamma < 0$ dB or $\alpha > 0$ dB and $\gamma > 0$ dB), the ratio Γ is between 5 dB and 6 dB.

In a two-mode laser, if one mode is stronger than the other one, the lowest mode is nearer threshold than the strongest one. According to figure 1, the lowest mode should therefore exhibit a higher RIN and we are therefore in the case $\alpha < 0$ dB and $\gamma > 0$ dB or $\alpha > 0$ dB and $\gamma < 0$ dB. Consequently, in a two-mode laser, we are probably always in the situation where an increase of more than 6 dB of Γ can be observed.

To conclude on this part, we have proposed an analytical description of the increase of the RIN of a two-mode laser after frequency-doubling. We have shown that the increase may be more than 6 dB. This situation occurs when the weakest mode exhibits the highest RIN. The reason is given by equation (26) and can be explained as follows. Through the SHG process, the nonlinear medium induces a coupling between the fluctuations of one mode and the average power of the other mode. This enhances the contribution of the highest RIN and may lead to an increase of more than 6 dB of the total RIN.

The analytical study proposed in this section is difficult to extend to a laser with more than two modes. In the following, we present some numerical results to study the effect of SHG on the RIN of a multimode fiber laser.

3. Numerical simulations of the multimode fiber laser

In the previous section, we have proposed an analytical study of the frequency-doubled RIN in the simple case of a two-mode laser. Studying the frequency-doubled RIN in the more general case of multimode laser (with any number of modes), requires a model that allows to simulate the time evolution of the electric field of each mode.

In multimode fiber lasers, modeling the dynamics of modes requires to include the effect of the spatial hole burning to take the mode competition into account. Such models have been developed [12, 13] but do include noise. On the other hand, models in which noise is taken into account through Langevin forces are commonly used in semiconductor lasers studies [14, 15] but do not include the spatial hole burning. To address this lack, we have developed a theoretical model to describe, as realistically as possible, the dynamics of a multimode fiber laser in the presence of intensity noise and mode competition. Solving numerically this model gives access to the output field $E_\omega(t)$ of the laser and allows us to calculate its RIN. Then, by taking the square of this field, we will be able to calculate the RIN of the laser after the SHG process.

In this section, we present the model we have developed and give an example of calculated RIN of the fundamental field of a typical multimode fiber laser. In the next section we will use the model to study the RIN of the frequency-doubled laser.

3.1. Equations of the model

The laser model is based on the semi-classical theory of class-B lasers [16]. For a single-mode laser, this theory leads to a set of two time-dependent first-order differential equations, describing the time evolution of the population inversion ΔN of the amplifying medium and the photon number S of the laser radiation. In the case of a multimode laser (with a number $N+1$ of modes for example), each mode of frequency ν_q (with $q = -N/2,\ldots,N/2$) should be described independently by its photon number S_q. In the case of fiber lasers, for a realistic description of the dynamics of the laser, the mode competition has to be taken into account. This is done through the spatial hole burning effect, which consists to expand the population inversion in Fourier series ΔN_q [12, 13]. Finally, to take noise into account, Langevin forces are added to each equation [14, 15]. The Langevin forces added to the population inversion equations represent the pump noise while the Langevin forces added to the photon number equations represent the spontaneous emission noise. Then, starting from the semi-classical theory of

the laser, and by including rigorously all the previously mentioned phenomena, we have obtained the set of the following equations

$$\frac{\mathrm{d}\Delta N_{\emptyset}(t)}{\mathrm{d}t} = \frac{1}{\tau}(\Delta N_{Pp} - \Delta N_{\emptyset}(t)) - \sum_q K_q S_q(t) \left(\Delta N_{\emptyset}(t) - \frac{1}{2}\Delta N_q(t) \right) + F_{\Delta N_{\emptyset}}(t), \tag{31}$$

$$\frac{\mathrm{d}\Delta N_q(t)}{\mathrm{d}t} = -\frac{1}{\tau}\Delta N_q(t) + K_q S_q(t)\Delta N_{\emptyset}(t) - \sum_l K_l S_l(t)\Delta N_l(t) + F_{\Delta N_q}(t), \tag{32}$$

$$\frac{\mathrm{d}S_q(t)}{\mathrm{d}t} = -\gamma_q S_q(t) + 2K_q \left(S_q(t) + 1 \right) \left(\Delta N_{\emptyset}(t) - \frac{1}{2}\Delta N_q(t) \right) + F_{S_q}(t). \tag{33}$$

The population inversion $\Delta N_{\emptyset}$ is the average population inversion (common to each mode) while $\Delta N_q(t)$ is the population inversion associated to each mode. The time τ is the lifetime of the laser upper level transition and γ_q is the inverse of this lifetime, estimated by [16]

$$\gamma_q^{-1} = -\frac{2L}{c\ln(R_1 R_2(\nu_q))}, \tag{34}$$

where L is the cavity length and R_1 and R_2 the reflection coefficients of the mirrors of the Fabry-Perot cavity. The parameter ΔN_{Pp} is the population inversion due to the pumping process. The coefficient K_q describes the amount of stimulated emission coupled to the qth mode. It is defined as [16]

$$K_q = \frac{\omega_q}{\varepsilon_0}\frac{\kappa}{\Delta\omega_a}\frac{1}{1+\left[\dfrac{2(\omega_q-\omega_a)}{\Delta\omega_a}\right]^2}, \tag{35}$$

where ω_a is the central frequency of the gain curve and $\Delta\omega_a$ the full-width at half maximum of the gain curve. The coupling constant κ comes from the scalar susceptibility for a homogeneously-broadened Lorentzian transition, defined by [16]

$$\kappa = \frac{3\varepsilon\lambda^3\omega_a\gamma_{\mathrm{rad}}}{4\pi^2}, \tag{36}$$

where ε is the permittivity, $\lambda = 2\pi c/\omega$ the wavelength, and γ_{rad} the radiative decay rate of the atomic transition given by [16]

$$\gamma_{\mathrm{rad}} = \frac{q_e\omega_a^2}{6\pi\varepsilon_0 m_e c^3}, \tag{37}$$

where q_e is the electron charge and m_e its mass.

Langevin forces $F_{\Delta N_\emptyset}$, $F_{\Delta N_q}$, and F_{S_q} are added to each equation. The magnitude of the Langevin forces is defined as follows [17, 18]

$$F_{\Delta N_\emptyset}(t) = \sqrt{\frac{D_{\Delta N_\emptyset \Delta N_\emptyset}}{\Delta t}} x_{\Delta N}(t), \tag{38}$$

$$F_{\Delta N_q}(t) = \sqrt{\frac{D_{\Delta N_q \Delta N_q}}{\Delta t}} x_{\Delta N}(t), \tag{39}$$

$$F_{S_q} = \sqrt{\frac{D_{S_q S_q}}{\Delta t}} x_{S_q}(t), \tag{40}$$

where Δt is the sampling time used in the numerical simulation, $D_{\Delta N_\emptyset \Delta N_\emptyset}$, $D_{\Delta N_q \Delta N_q}$, and $D_{S_q S_q}$ are the diffusion coefficients and $x_{\Delta N}(t)$ and $x_{S_q}(t)$ are independent Gaussian random variables with a zero mean value and a variance of unity. The random variable $x_{\Delta N}(t)$, that appears in the inversion population equations (38) and (39), can be attributed to pump noise while the random variable $x_{S_q}(t)$ is due to spontaneous emission. These stochastic terms are numerically generated by computer random numbers. Let us precise that, in our approach, we only consider noise sources such as pump noise and spontaneous photon emission. External phenomena, such as acoustic vibrations for example, are not taken into account. The diffusion coefficient $D_{\Delta N_q \Delta N_q}$ is related to $D_{\Delta N_\emptyset \Delta N_\emptyset}$ by the following relation

$$D_{\Delta N_q \Delta N_q} = \left(\frac{K_q}{K_0}\right)^2 D_{\Delta N_\emptyset \Delta N_\emptyset}. \tag{41}$$

3.2. Studied fiber laser

We will know apply the previously described model to a standard fiber laser. We consider the Yb-doped fiber laser described in figure 3. The fiber of length L is pumped at 915 nm by a laser diode. The fiber laser cavity is formed by two fiber Bragg gratings (FBGs) around 1064 nm. Their reflection coefficients for the intensity are respectively R_1 and R_2. The output laser field $E_\omega(t)$ around 1064 nm propagates in a second-order nonlinear medium (a periodically-poled lithium niobate crystal for example) and creates a new green laser field $E_{2\omega}(t)$ at 532 nm through the SHG process.

The reflectivity R_1 of the input FBG is assumed to be 100 % over a large bandwidth. In the following, we will have to consider the frequency dependence of the reflectivity R_2 of the output FBG. For simplicity, we assume a Gaussian

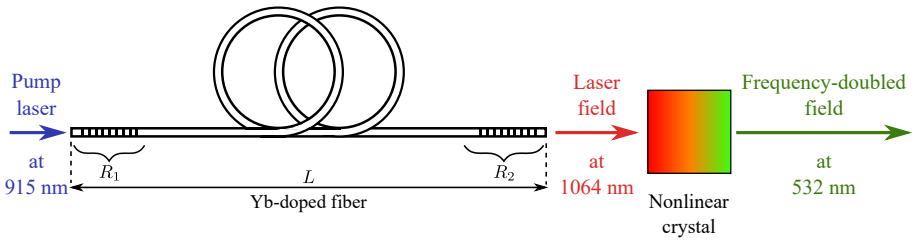

Figure 3: Schematic representation of the studied Yb-doped fiber laser.

shape

$$R_2(\nu) = R_{2\mathrm{Max}} e^{-\dfrac{(\nu-\nu_0)^2}{\Delta\nu^2}}, \tag{42}$$

where $R_{2\mathrm{Max}}$ is the maximum reflectivity of the grating, ν_0 its central frequency (its corresponding central wavelength is $\lambda_0 = c/\nu_0$) and $\Delta\nu$ its half-width at $1/e$ of the maximum reflectivity.

3.3. Numerical simulations

The model (31)–(33), applied to the previous fiber laser, is numerically solved in order to obtain the time evolution of the number of photons $S_q(t)$ of each mode. From $S_q(t)$, the field $E_q(t)$ of each mode is calculated as follows

$$E_q(t) = \sqrt{S_q(t)} e^{i\omega_q t}. \tag{43}$$

The total laser field is the sum of each individual field

$$E_\omega(t) = \sum_{q=-N/2}^{N/2} E_q(t). \tag{44}$$

The total intensity $I_\omega(t)$ of the multimode fiber laser and the intensity $I_q(t)$ of each mode are calculated from $E_\omega(t)$ and $E_q(t)$, respectively, using equation (1). It is numerically straightforward to decompose $I_\omega(t)$ in its average value $\langle I_\omega \rangle$ and in its time-dependent fluctuations $\delta I_\omega(t)$ similarly to equation (2). The RIN of the multimode laser is then calculated using equation (3). Similarly, the intensity $I_q(t)$ of each mode is decomposed in its average value $\langle I_q \rangle$ and in its time-dependent fluctuations $\delta I_q(t)$. We can therefore calculate the noise of each mode by calculating its PSD $\langle |\widetilde{\delta I}_q(\nu)|^2 \rangle$. However, instead of dividing the PSDs by the square of the average intensity $\langle I_q \rangle^2$ of each mode (which would gives

the RIN of each mode), we divide all the individual PSDs by the same quantity, namely the square of the total average intensity $\langle I_\omega \rangle^2$. This leads to what we call the normalized power spectral density $\overline{\mathrm{PSD}}_q(\nu)$ of each mode

$$\overline{\mathrm{PSD}}_q(\nu) = \frac{\langle |\tilde{\delta I}_q(\nu)|^2 \rangle}{\langle I_\omega \rangle^2}. \tag{45}$$

This quantity is more convenient to compare between themselves the fluctuations of each mode.

Using these definitions we are able to plot the RIN of the multimode laser and the normalized PSDs of each mode. The parameters we used in the model are summarized in table 1. The model is solved using Matlab and a 4th-order Runge–Kutta method. The fast Fourier transform algorithm is used to plot the PSDs from the time evolution of the intensities. The pump power is set to 100 mW and the output laser power is around 5 mW.

Parameter	Symbol	Value	Unit
Cavity length	L	5	m
Front mirror reflectivity	R_1	1	
Output mirror reflectivity at central wavelength	$R_{2\mathrm{Max}}$	0.8	
Mode effective index	n	1.47	
Ion concentration	N_t	10^{23}	m^{-3}
Central wavelength	λ_0	1064	nm
Free spectral range	$\delta\nu$	20	MHz
Gain spectral width	$\Delta\nu_a$	10	THz
Lifetime of the upper level transition	τ	840	μs
Spectral width of the output FBG	$\Delta\nu$	2	GHz
Diffusion coefficient of the normalized population inversion $\Delta N_\emptyset$	$D_{\Delta N_\emptyset \Delta N_\emptyset}$	10^{-6}	
Diffusion coefficient of the qth photons number S_q	$D_{S_q S_q}$	10^{-9}	

Table 1: Values of the parameters used in the model.

The numerical resolution of the model is quite time and memory consuming, in particular if we consider a large number of modes and a broad frequency range for the RIN. In the following, and with no loss of generality, we will limit our simulation to a laser with 9 modes and to a frequency range of 1kHz-100MHz.

Figure 4 shows the RIN spectrum of the 9-mode fiber laser (black curve). The normalized PSDs of the 9 modes are also plotted (color curves). The total RIN of the 9-mode laser exhibits an excess noise just above -120 dB/Hz at low frequencies, a relaxation frequency peak at 50 kHz and several high-frequency peaks. These high-frequency peaks correspond to the beating frequency at the FSR $\delta\nu$ of the cavity and its harmonics. They are due to the cross products generated when the modulus of the sum of the fields [equation (44)] is squared in order to calculate the total intensity. Since the number of modes considered in this example is 9, we have 8 beating frequencies in figure 4. Note that the simulated total RIN presented in 4 is similar to the RINs that can be measured experimentally in standard multimode fiber lasers.

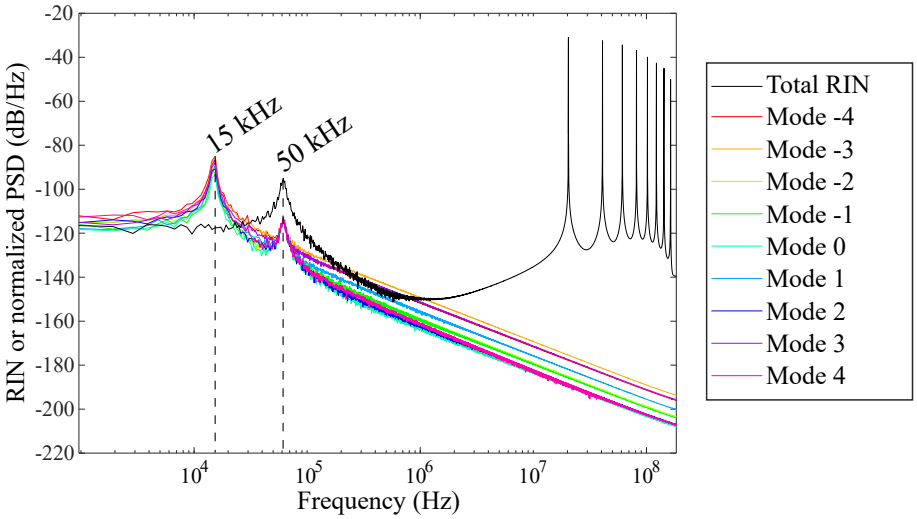

Figure 4: Laser RIN of a 9-mode fiber laser (in black) and normalized PSDs of each mode (in colors).

The normalized PSDs are also reported in figure 4 for each mode and have a different behavior. First, they do not exhibit the beating high frequencies visible on the total RIN. Since these beating frequencies are due to the cross products generated by the calculus of the total intensity, they cannot appear for individual modes. Secondly, if the relaxation frequency peak at 50 kHz is still visible on each normalized PSD, a new peak at 15 kHz occurs. This peak is due to the antiphase dynamics of the mode competition. This phenomenon is well-known in multimode lasers [13, 19, 20]. This peak corresponds to the frequency at which modes exchange energy due to cross-saturation dynamics. This peak is visible on the noise spectrum of each individual mode. When the mode intensities are

similar, the antiphase dynamics of mode competition leads to the cancellation of the fluctuations when the total RIN is considered [13]. Note that this occurs only if the intensities of modes are similar.

We also note that all individual PSDs have approximately the same level of noise. Indeed, with a spacing between modes of 20 MHz and a bandwidth of the output FBG of 2 GHz (see table 1), all the modes have approximately the same losses and, consequently, the same noise.

To conclude on this part, we have established the model (31)–(33) to describe the dynamics of a multimode fiber laser with intensity noise. The numerical resolution of the model has allowed us to plot the PSDs of individual modes and the total RIN of the laser. This model is, at the best of our knowledge, an original model including spatial hole burning (to take mode competition into account) and Langevin forces (to take noise into account). It allows to simulate the complex amplitude of each mode to calculate both the individual RINs and the total RIN of the laser. In the following, we will apply this model to study the RIN of a frequency-doubled multimode fiber laser.

4. RIN of the frequency-doubled multimode laser

In this part, we use our model to numerically calculate the total electric field of a multimode fiber laser. By raising this field to the power of 2, we will obtain the electric field of the frequency-doubled laser. Then, we will be able to compare the RIN of the laser before and after the frequency-doubling operation. In order to compare the results with the analytical study of Section 2, we start with a two-mode laser. Then, we will investigate a laser with a larger number of modes.

4.1. Two-mode laser

We first consider the set of equations (31)–(33) with only two modes at two different frequencies. The physical parameters of the laser are the same than in table 1 (except for the spectral width of the output FBG, as we will see below). The optical frequency of one mode coincides with the central frequency of the output FBG, the other frequency is up-shifted by the FSR value (20 MHz in our case).

Two different values of the output FBG bandwidth are considered in the following. Figure 5 plots the reflectivity of both FBGs as a function of the optical frequency, assuming a Gaussian shape [equation (42)]. One value of the bandwidth is 2 GHz. With this value, we can consider that both modes lie in the vicinity of the maximum reflectivity of the grating (see figure 5) and experience

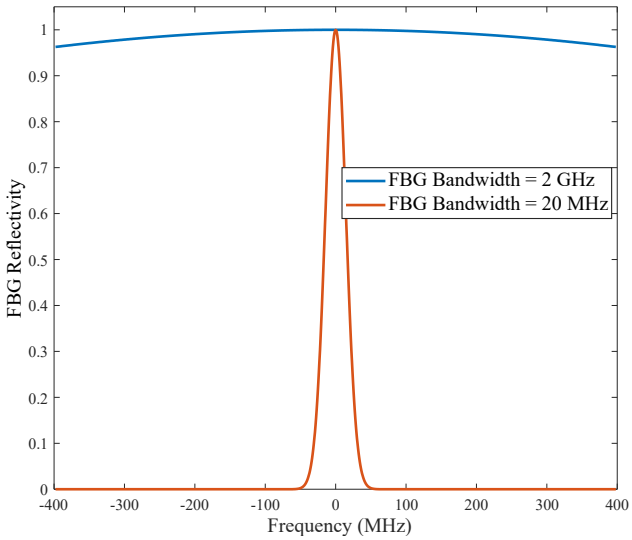

Figure 5: Reflectivities of the two output FBGs considered in our study.

approximately the same losses. In this case, both modes have the same average intensity ($\alpha = 0$ dB) and the same RIN ($\gamma = 0$ dB). This case corresponds to point (I) in figure 2. The second case corresponds to a bandwidth of the output FBG of 20 MHz. Although this small value is not achievable for real FBGs, it allows us to take into account different reflectivities, i.e. different losses, for both modes. As a consequence, they have different average intensities and different RINs. In this case, the ratio between the average intensities of both modes is $\alpha = -6$ dB and the ratio between their RIN is $\gamma = 20$ dB. This case corresponds to point (II) in figure 2. Note that these values of α and γ have been obtained after having solved numerically the model and confirm that we are in the case where the mode with the lowest intensity exhibits the highest RIN.

Figure 6(a) shows the calculated RINs of the two-mode laser before (black curve) and after (green curve) frequency-doubling in the case of point (I) of figure 2. According to the analytical study of Section 2, we confirm a 6 dB increase of the low-frequency RIN. In the following, we will define the low-frequency RIN as the RIN over a frequency range below the relaxation peak [50 kHz in the case of figure 6(a)]. We also observe that, according to equation (14), the RIN at frequency ω exhibits only one frequency peak at the FSR while the RIN at 2ω exhibits, according to equation (22), two frequency peaks: one at the FSR and the second one at twice the FSR. Finally, we note that no low-frequency peak due to the mode competition is visible on both RINs. Indeed, as mentioned in Section

3.3, the antiphase behavior of the dynamics of both individual modes leads to the cancellation of this peak on the total RIN, especially when the modes have the same intensity.

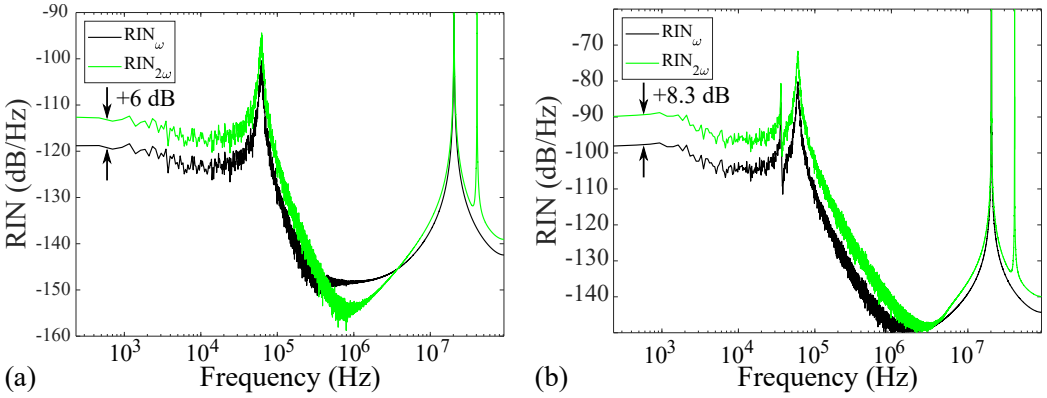

Figure 6: Numerical simulation of RINs of a two-mode fiber laser before and after frequency doubling. (a) $\alpha = 1$ et $\gamma = 0$ dB [point (I) of figure 2] ; (b) $\alpha = 0,25$ et $\gamma = 20$ dB [point (II) of figure 2].

Figure 6(b) shows the calculated RIN spectra, before and after frequency doubling, when the average intensities of both modes are different, corresponding to point (II) of figure 2. We immediately observe that the increase of the low-frequency RIN is 8.3 dB, instead of 6 dB, like in the previous case. This value is in perfect accordance with the value of Γ obtained from figure 2 at point (II). These observations confirm the validity of both the analytical approach presented in Section 2.2 and the multimode laser model we have presented in Section 3.1.

The main result here is that the frequency doubling operation can lead to an increase of the RIN of more than 6 dB at low frequencies for a two-mode laser, unlike a single-mode laser for which the increase is only 6 dB. This situation occurs when the mode with the lowest intensity exhibits the highest RIN, which is the case for this two-mode laser.

We also observe in figure 6(b) that the antiphase peak is visible at 40 kHz on both the RIN before and the RIN after frequency doubling. Let us recall that this peak, visible on each individual RIN, is due do energy exchanges between modes. When modes have the same intensity, the peak vanishes when the total RIN is plotted, because of the antiphase dynamics [13]. Here, modes have different intensities and their sum does not compensate the antiphase dynamics. Therefore, an oscillation remains on both the total RIN and the frequency-doubled RIN.

Let us now consider a fiber laser with a larger number of modes.

4.2. 15-mode laser

In this part, we numerically solve our model with 15 modes. This number of modes is much below the number of modes of a real fiber laser, which could be of the order of one thousand for example. Here, we deliberately limit the number of modes to save computational time and memory, with no loss of generality. The parameters used in the simulation are the same than in table 1. Similarly to the previous section, we consider two different values of the output FBG bandwidth. This allows us to simulate two cases. In the first case, with a large FBG bandwidth of 2 GHz, all the modes have approximately the same intensity. In the second one, with a narrower FBG bandwidth of 40 MHz, the modes experience different losses and have different output intensities.

Figure 7(a) plots the calculated RIN before and after frequency doubling in the first case (same intensity for all modes) and figure 7(b) plots the RINs in the second case (different intensities for the modes).

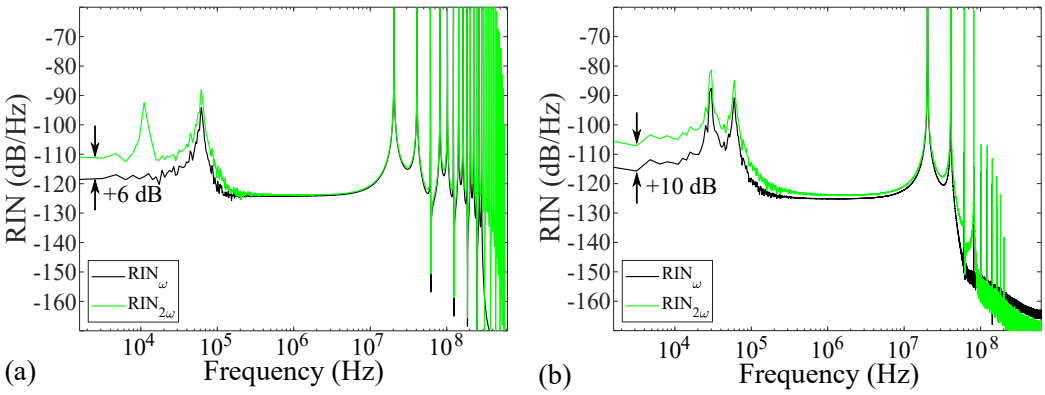

Figure 7: Numerical simulation of RINs of a 15-modes laser before and after frequency doubling. (a) Case of 15 modes with the same average intensity and the same RIN ; (b) case of 15 modes with the different average intensities and RINs.

In figure 7(a), we observe that the increase of the RIN, due to frequency doubling, is 6 dB at low-frequency. This is in accordance with the analytical two-mode-laser study of Section 2 where we have shown that the increase of the low-frequency RIN is 6 dB when the mode intensities are the same. We note in this figure the larger number of beating frequencies at the FSR and its harmonics, due to the larger number of modes considered in this study.

We also observe a new phenomenon in figure 7(a). An antiphase peak at 10 kHz is visible on the frequency-doubled RIN while it does not appear on the initial RIN. As explained in more details in Appendix A, this new phenomenon starts

to be visible when the number of modes is greater than two. This is due to new cross products in the frequency-doubled intensity that avoid the antiphase low-frequency peak to be cancelled out. Let us point out that the observation of this new phenomenon is made possible because our model takes into account the mode competition in the fiber laser.

In figure 7(b), when the 15 modes have different average intensities and RINs, the increase of the low-frequency RIN is 10 dB. Similarly to the two-mode case described in Section 4.1, this increase of more than 6 dB is attributed to a transfer of noise from modes with higher RINs to modes with higher intensities, accordingly with our analytical study of Section 2.

In figure 7(b), we also observe that the number of high-frequency peaks at the FSR and its harmonics is smaller than in figure 7(a). Indeed, with a narrower output FBG, some modes have less intensity than the others and some modes (farthest away from the central frequency of the FBG) are even below threshold. In this case, the number of modes that really contribute to the laser field is less than 15.

Finally, we observe in figure 7(b) that an antiphase peak at 30 kHz remains visible even on the initial RIN. As already discussed in Section 4.1, this is explained by the fact that, when mode intensities are different in a multimode laser, the antiphase behavior cannot be cancelled out on the total intensity. The frequency at which energy exchange occurs, remains therefore visible on the RIN spectrum of the laser.

In this section, we have presented numerical simulations of the model described Section 3 to study the RIN evolution of a multimode fiber laser before and after a frequency-doubling operation. We have investigated two cases: a two-mode laser and a 15-mode laser. In both cases, the numerical results have confirmed the theoretical prediction of Section 2: after frequency-doubling, an increase of the RIN of more than 6 dB is obtained if the modes experience different intensities and, consequently, different RINs. We have limited our study to a maximum of 15 modes to limit the computational time but this approach may be, in principle, extended to a larger number of modes.

5. Conclusion

In this work we have proposed a theoretical explanation of a phenomenon that has already been experimentally observed in frequency-doubled lasers: an increase of more that 6 dB of the low-frequency RIN after the frequency-doubling operation. Our approach has been very simple. We have just considered the SHG

as the squaring of a multimode electric field. We have started our study with a two-mode laser and have been able to propose an analytical formula proving that an increase of more tan 6 dB is possible when the two-mode laser is frequency doubled. We have shown that this only occurs if both modes have different intensities and if the mode with the lowest intensity has the highest RIN. This is explained by the coupling, trough the nonlinear medium, between the fluctuations of the nosiest mode with the intensity of the highest mode.

Since this analytical approach is not easily transposable to a larger number of modes, we have developed a theoretical model to describe the dynamics of a multimode fiber laser with noise. To properly described the multimode fiber laser, the model includes noise sources (through Langevin forces) but also the spatial hole burning effect which plays a major role in the dynamics of multimode fiber lasers.

By solving numerically this model, we have been able to square the electric field of the multimode fiber laser and study the evolution of the RIN before and after frequency doubling. We have first numerically simulate a two-mode laser to compare the results with our analytical study. Then we have studied a 15-mode laser. Our numerical results have confirmed that an increase of the low-frequency RIN is obtained when the modes have different intensities while an increase of only 6 dB is obtained when all mode intensities are equal, according to our analytical prediction.

In multimode fiber lasers, and more generally in any multimode lasers, the modes that experience more losses than the others are nearer threshold and experience a higher RIN. As a consequence, and according to the theory we have developed in this paper, a frequency-doubled multimode laser will always exhibit a low-frequency RIN 6 dB higher than the RIN of the laser at the fundamental frequency. This result could explain the increase of the excess noise observed experimentally in some frequency-doubled laser architectures.

This paper has also been the occasion to present an original model to study the dynamics of a multimode fiber laser with noise. This model has been successfully used to study a frequency-doubled laser. It has also highlighted the possibility to study some behaviors of the laser related to the antiphase dynamics of mode competition. This model may also be of great interest for dynamical studies of multimode fiber lasers outside the scope of SHG.

Let us now point out some possible perspectives of this work. First, extending this work to more realistic systems with larger numbers of modes would be very relevant. This would require computational powers that are relatively easily achievable today. The model we have developed and presented in this paper does

not take the phase noise into account. It could be judicious to add an equation for the phase into the model to study the possible coupling between phase and intensity noise through the nonlinear medium. Our approach should be valid for any kind of fiber lasers and it would be interesting to theoretically study the influence of different parameters of laser systems, such as laser output power, length of doped fiber, FBG bandwidths, parameters of SHG crystals, etc. Finally, it would be very interesting to compare these theoretical results to experimental ones. It would allow to test the validity of the different hypothesis we made to develop our approach.

6. Acknowledgments

The authors would like to thank the French *Direction Générale de l'Armement* (DGA) and *Lannion Trégor Communauté* (LTC) for their financial support of this work.

Appendix A. Intensity calculation of a frequency-doubled 3-mode laser

The aim of this appendix is to understand the presence of the antiphase low-frequency peak on the RIN of the frequency-doubled 15-mode laser in figure 7(a). To this end, we provide details of the calculation of the intensity of a 3-mode laser after frequency doubling. We will show that, from a number of modes equal to 3, new terms in the frequency-doubled intensity are responsible for the presence of the antiphase peak.

Using the same method than in Section 2.2, we write the total electric field $E_\omega(t)$ as the sum of 3 electric fields $E_1(t)$, $E_2(t)$ and $E_3(t)$ at three adjacent frequencies of the Fabry-Perot cavity

$$E_\omega(t) = E_1(t) + E_2(t) + E_2(t). \tag{A.1}$$

The electric field of each mode is expressed as in equation (11). To calculate the frequency-doubled intensity $I_{2\omega}(t)$, we first square the electric field $E_\omega(t)$ to obtain the frequency-doubled field $E_{2\omega}(t)$ [equation (4)]. Then, by taking the modulus square of $E_{2\omega}(t)$ [equation (5)], we obtain $I_{2\omega}(t)$

$$
\begin{aligned}
I_{2\omega}(t) =& \eta \Big[I_1^2(t) + I_2^2(t) + I_3^2(t) + 4I_1(t)I_2(t) + 4I_1(t)I_3(t) + 4I_2(t)I_3(t) \\
&+ 4I_2(t)\sqrt{I_1(t)I_3(t)} \\
&+ 4I_1(t)\sqrt{I_1(t)I_2(t)}\cos(\delta\omega t) + 8I_1(t)\sqrt{I_2(t)I_3(t)}\cos(\delta\omega t) \\
&+ 4I_2(t)\sqrt{I_1(t)I_2(t)}\cos(\delta\omega t) + 8I_3(t)\sqrt{I_1(t)I_2(t)}\cos(\delta\omega t) \\
&+ 4I_2(t)\sqrt{I_2(t)I_3(t)}\cos(\delta\omega t) + 4I_3(t)\sqrt{I_2(t)I_3(t)}\cos(\delta\omega t) \\
&+ 4I_1(t)\sqrt{I_1(t)I_3(t)}\cos(2\delta\omega t) + 2I_1(t)I_2(t)\cos(2\delta\omega t) \\
&+ 8I_2(t)\sqrt{I_1(t)I_3(t)}\cos(2\delta\omega t) + 4I_3(t)\sqrt{I_1(t)I_3(t)}\cos(2\delta\omega t) \\
&+ 2I_2(t)I_3(t)\cos(2\delta\omega t) \\
&+ 4I_1(t)\sqrt{I_2(t)I_3(t)}\cos(3\delta\omega t) + 4I_3(t)\sqrt{I_1(t)I_2(t)}\cos(3\delta\omega t) \\
&+ 2I_1(t)I_3(t)\cos(4\delta\omega t) \Big], \qquad \text{(A.2)}
\end{aligned}
$$

where $I_1(t)$, $I_2(t)$ and $I_3(t)$ are the intensities of each mode and $\delta\omega$ the FSR of the cavity. We suppose that the RIN of each mode is similar to the RIN of a single-mode laser, as shown in figure 1 for example.

In expression (A.2), we can define three different contributions: $I_{2\omega\mathrm{lf}}$ at low-frequency, $I_{2\omega\mathrm{hf}}$ at high-frequency, and $I_{2\omega\mathrm{cp}}$ for a new term, corresponding to a new cross product. These contributions write

$$
I_{2\omega\mathrm{lf}}(t) = \eta\,[I_1^2(t) + I_2^2(t) + I_3^2(t) + 4I_1(t)I_2(t) + 4I_1(t)I_3(t) + 4I_2(t)I_3(t)], \qquad \text{(A.3)}
$$

$$
\begin{aligned}
I_{2\omega\mathrm{hf}}(t) =& \eta \Big[4I_1(t)\sqrt{I_1(t)I_2(t)}\cos(\delta\omega t) + 8I_1(t)\sqrt{I_2(t)I_3(t)}\cos(\delta\omega t) \\
&+ 4I_2(t)\sqrt{I_1(t)I_2(t)}\cos(\delta\omega t) + 8I_3(t)\sqrt{I_1(t)I_2(t)}\cos(\delta\omega t) \\
&+ 4I_2(t)\sqrt{I_2(t)I_3(t)}\cos(\delta\omega t) + 4I_3(t)\sqrt{I_2(t)I_3(t)}\cos(\delta\omega t) \\
&+ 4I_1(t)\sqrt{I_1(t)I_3(t)}\cos(2\delta\omega t) + 2I_1(t)I_2(t)\cos(2\delta\omega t) \\
&+ 8I_2(t)\sqrt{I_1(t)I_3(t)}\cos(2\delta\omega t) + 4I_3(t)\sqrt{I_1(t)I_3(t)}\cos(2\delta\omega t) \\
&+ 2I_2(t)I_3(t)\cos(2\delta\omega t) \\
&+ 4I_1(t)\sqrt{I_2(t)I_3(t)}\cos(3\delta\omega t) + 4I_3(t)\sqrt{I_1(t)I_2(t)}\cos(3\delta\omega t) \\
&+ 2I_1(t)I_3(t)\cos(4\delta\omega t) \Big], \qquad \text{(A.4)}
\end{aligned}
$$

$$
I_{2\omega\mathrm{cp}} = 4I_2(t)\sqrt{I_1(t)I_3(t)}. \qquad \text{(A.5)}
$$

As stated previously in Section 2 for two modes, the low-frequency term $I_{2\omega\mathrm{lf}}$ has it main contribution on the total RIN at low frequencies (typically below 1 MHz). The contribution of the high-frequency term $I_{2\omega\mathrm{hf}}$ on the total RIN consists in high-frequency peaks at the FSR and its harmonics (until $4\delta\omega$ in the present case). The cross-product term $I_{2\omega\mathrm{cp}}$ has also its contribution on the total RIN at low frequencies because it depends only on the three intensities and does not include any beating terms. However, this term writes quite differently than the terms in $I_{2\omega\mathrm{lf}}$ and will be treated separately.

Using our numerical model for three modes, we have been able to reconstruct the three contributions $I_{2\omega\mathrm{lf}}$, $I_{2\omega\mathrm{hf}}$ and $I_{2\omega\mathrm{cp}}$. In the model we have considered three modes with the same intensity. Figure A.8 plots the RIN of these three terms together with the RIN of the total intensity $I_{2\omega}$. We clearly see that the RIN of $I_{2\omega\mathrm{lf}}$ is similar to the RIN of a single-mode laser exhibiting an excess noise floor at low frequencies and a relaxation peak at 70 kHz. On the RIN of $I_{2\omega\mathrm{hf}}$, we observe the high-frequency peaks at the FSR and its harmonics, as expected from equation (A.4). The interesting phenomenon comes from the RIN contribution of $I_{2\omega\mathrm{cp}}$. On this RIN, we observe a new peak at 24 kHz, corresponding to the antiphase peak due to mode competition. Actually, this peak is visible on the individual RIN of each fundamental intensity $I_i(t)$ (with $i = 1,2,3$) and each frequency-doubled intensity $I_i^2(t)$ (not plotted in figure A.8). This peak corresponds to the frequency at which the three modes exchange energy due to the mode competition. In the time domain, this leads to an oscillation of the intensity of each mode. Because of its antiphase nature, and only if the mode intensities are of the same order of magnitude, this oscillation disappears when the sum of the fundamental intensities $I_1(t) + I_2(t) + I_2(t)$ is considered, as already pointed out in Section 3 (figure 4) and Section 4 (figure 6). We see from figure A.8 that the oscillation also vanishes on the low-frequency contribution $I_{2\omega\mathrm{lf}}$ of the frequency-doubled intensity. This is explained by the fact that, in the expression (A.3) of $I_{2\omega\mathrm{lf}}$, all the individual intensities have the same weight. The oscillations on each individual mode can therefore compensate each other. With three modes, the frequency-doubled intensity $I_{2\omega}$ of the laser reveals the new contribution $I_{2\omega\mathrm{cp}}$. This term has not a mathematical form allowing the antiphase oscillations of modes to compensate each other. Thus, the antiphase peak is clearly visible on the RIN of $I_{2\omega\mathrm{cp}}$ in figure A.8 and, then, on the RIN of the total intensity $I_{2\omega}$.

To summary this part, we have shown that the antiphase peak cannot disappear on the RIN of a the frequency-doubled 3-mode laser, even if the intensities of the modes are equal. This is due to the additional low-frequency contribution $I_{2\omega\mathrm{cp}}$. This term is generated by the nonlinear coupling between three modes due to

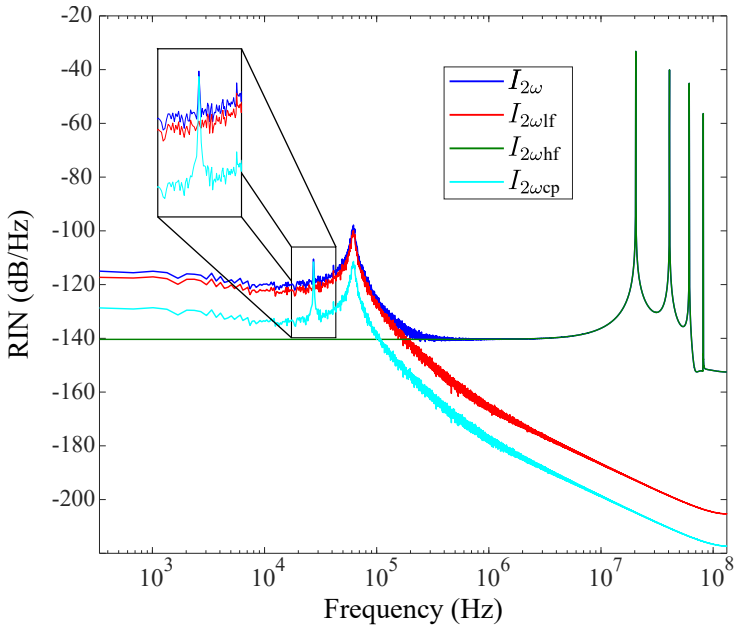

Figure A.8: Numerical simulation of the RIN of a frequency-doubled 3-modes laser and its decomposition in different intensity contributions.

SHG. From a number of modes equal or greater than three, this term is always present and its complexity increases with the number of modes. For example, for a 4-mode laser, this term is equal to

$$I_{2\omega\mathrm{cp}}^{4\mathrm{modes}} = 4I_2(t)\sqrt{I_1(t)I_3(t)} + 4I_3(t)\sqrt{I_2(t)I_4(t)} + 8\sqrt{I_1(t)I_2(t)I_3(t)I_4(t)}. \quad \text{(A.6)}$$

In this appendix, we have shown that, in a frequency-doubled multimode laser (from a number of modes ≥ 3), due to the SHG process, the low-frequency contribution of mode competition systematically appears on the RIN of the laser.

References

[1] D. J. Richardson, J. Nilsson, W. A. Clarkson, High power fiber lasers: current status and future perspectives, J. Opt. Soc. Am. B 27 (2010) B63–B92.

[2] P. A. Champert, S. V. Popov, J. R. Taylor, J. P. Meyn, Efficient second-harmonic generation at 384 nm in periodically poled lithium tantalate by use of a visible Yb–Er-seeded fiber source, Opt. Lett. 25 (2000) 1252–1254.

[3] P. Dupriez, J. K. Sahu, A. Malinowski, Y. Jeong, D. J. Richardson, J. Nilsson, 80 W green laser based on a frequency-doubled picosecond, single-mode, linearly-polarized fiber laser, in: Conference on Lasers and Electro-Optics, Optical Society of America, 2006, p. CThJ1.

[4] J. Zhang, H. Chang, X. Jia, H. Lei, R. Wang, C. Xie, K. Peng, Suppression of the intensity noise of a laser-diode-pumped single-frequency ring Nd:YVO4–KTP green laser by optoelectronic feedback, Opt. Lett. 26 (2001) 695–697.

[5] A. E. Amili, M. Alouini, Noise reduction in solid-state lasers using a SHG-based buffer reservoir, Opt. Lett. 40 (2015) 1149–1152.

[6] U. Eismann, M. Enderlein, K. Simeonidis, F. Keller, F. Rohde, D. Opalevs, M. Scholz, W. Kaenders, J. Stuhler, Active and passive stabilization of a high-power violet frequency-doubled diode laser, in: Conference on Lasers and Electro-Optics, Optical Society of America, 2016.

[7] M. Tawfieq, A. K. Hansen, O. B. Jensen, D. Marti, B. Sumpf, P. E. Andersen, Intensity Noise Transfer Through a Diode-Pumped Titanium Sapphire Laser System, IEEE Journal of Quantum Electronics 54 (2018) 1–9.

[8] R. Paschotta, Encyclopedia of Laser Physics and Technology, Wiley-VCH, 2008.

[9] E. Rosencher, B. Vinter, Optoelectronics, Cambridge University Press, 2002.

[10] R. Boyd, D. Prato, Nonlinear Optics, Nonlinear Optics Series, Elsevier Science, 2008.

[11] S. I. Kablukov, E. A. Zlobina, E. V. Podivilov, S. A. Babin, Output spectrum of yb-doped fiber lasers, Opt. Lett. 37 (2012) 2508–2510.

[12] C. L. Tang, H. Statz, G. deMars, Spectral output and spiking behavior of solid-state lasers, Journal of Applied Physics 34 (1963) 2289–2295.

[13] K. Otsuka, Multimode Laser Dynamics, Progress in Quantum Electronics 23 (1999) 97–129.

[14] M. Ahmed, M. Yamada, Influence of instantaneous mode competition on the dynamics of semiconductor lasers, IEEE Journal of Quantum Electronics 38 (2002) 682–693.

[15] M. Yamada, Theory of Semiconductor Lasers, Springer, Tokyo, 2014.

[16] A. E. Siegman, Lasers, University Science Books, Mill Valley, Calif, 1986.

[17] I. Fatadin, D. Ives, M. Wicks, Numerical simulation of intensity and phase noise from extracted parameters for cw dfb lasers, IEEE Journal of Quantum Electronics 42 (2006) 934–941.

[18] G. Baili, F. Bretenaker, M. Alouini, L. Morvan, D. Dolfi, I. Sagnes, Experimental investigation and analytical modeling of excess intensity noise in semiconductor class-a lasers, J. Lightwave Technol. 26 (2008) 952–961.

[19] S. Bielawski, D. Derozier, P. Glorieux, Antiphase dynamics and polarization effects in the Nd-doped fiber laser, Phys. Rev. A 46 (1992) 2811–2822.

[20] P. L. Boudec, C. Jaouen, P. L. François, J.-F. Bayon, F. Sanchez, P. Besnard, G. Stéphan, Antiphase dynamics and chaos in self-pulsing erbium-doped fiber lasers, Opt. Lett. 18 (1993) 1890–1892.